PROCEEDINGS OF SPIE

SPIEDigitalLibrary.org/conference-proceedings-of-spie

Random telegraph signal (RTS) noise and other anomalies in the near-infrared detector systems for the Euclid mission

Ralf Kohley, Rémi Barbier, Bogna Kubik, Sylvain Ferriol, Jean-Claude Clemens, et al.

Ralf Kohley, Rémi Barbier, Bogna Kubik, Sylvain Ferriol, Jean-Claude Clemens, Anne Ealet, Aurélia Secroun, Luca Conversi, Paolo Strada, "Random telegraph signal (RTS) noise and other anomalies in the near-infrared detector systems for the Euclid mission," Proc. SPIE 9915, High Energy, Optical, and Infrared Detectors for Astronomy VII, 99150H (5 August 2016); doi: 10.1117/12.2233352

SPIE.

Event: SPIE Astronomical Telescopes + Instrumentation, 2016, Edinburgh, United Kingdom

Random telegraph signal (RTS) noise and other anomalies in the near-infrared detector systems for the Euclid mission

Ralf Kohley*[a], Rémi Barbier[b], Bogna Kubik[b], Sylvain Ferriol[b], Jean-Claude Clémens[c], Anne Ealet[c], Aurélia Secroun[c], Luca Conversi[a], Paolo Strada[d]

[a]European Space Agency / ESAC, Camino Bajo del Castillo, 28692 Villanueva de la Cañada, Spain;
[b]Institut de Physique Nucléaire de Lyon (IPNL), 4, Rue Enrico Fermi, 69622 Villeurbanne, France;
[c]Centre de Physique des Particules de Marseille (CPPM), 163, avenue de Luminy, 13288 Marseille, France;
[d]European Space Agency / ESTEC, Keplerlaan 1, 2201 AZ Noordwijk, The Netherlands

ABSTRACT

Euclid is an ESA mission to map the geometry of the dark Universe with a planned launch date in 2020. Euclid is optimised for two primary cosmological probes, weak gravitational lensing and galaxy clustering. They are implemented through two science instruments on-board Euclid, a visible imager (VIS) and a near-infrared spectro-photometer (NISP), which are being developed and built by the Euclid Consortium instrument development teams. The NISP instrument contains a large focal plane assembly of 16 Teledyne HgCdTe H2RG detectors with 2.3µm cut-off wavelength and SIDECAR readout electronics. The performance of the detector systems is critical to the science return of the mission and extended on-ground tests are being performed for characterisation and calibration purposes. Special attention is given also to effects even on the scale of individual pixels, which are difficult to model and calibrate, and to identify any possible impact on science performance. This paper discusses a variety of undesired pixel behaviour including the known effect of random telegraph signal (RTS) noise based on initial on-ground test results from demonstrator model detector systems. Some stability aspects of the RTS pixel populations are addressed as well.

Keywords: RTS noise, RTN, Euclid, NISP, H2RG

1. INTRODUCTION

The combined focal plane for the Near-Infrared Spectrometer and Photometer (NISP) of the ESA medium class mission Euclid (see [1] and [2] for further details on the Euclid mission and NISP) consists of 16 individual detector systems called Sensor Chip Systems (SCS) arranged in an array of 4 by 4 SCS in the focal plane assembly (FPA). The SCS comprises a HgCdTe H2RG detector with 2.3µm cut-off wavelength called the Sensor Chip Assembly (SCA), a cryogenic flex cable (CFC) and the SIDECAR readout electronics called Sensor Chip Electronics (SCE). This triplet of SCA, CFC and SCE are custom made by Teledyne Imaging Sensors (TIS) for the Euclid mission and provided by NASA through JPL with characterisation and acceptance testing under responsibility of the Detector Characterization Laboratory (DCL) at Goddard Space Flight Center (GSFC).

ESA started in August 2012 a pre-development phase with TIS for the Euclid SCS. Some parts from this NRE phase were granted to the Euclid Consortium and implemented at the Laboratoire d'Astrophysique de Marseille (LAM) as part of the Demonstrator Model (DM) of the Euclid Focal Plane Array (FPA). The setup of the DM FPA is shown in Figure 1 and further details about the test can be found in [3].

The overall science performance of the SCS is excellent considering the statistical percentile of the over 4 million pixels. Each pixel can be considered an individual detector within the SCA with its own properties in terms of characteristics such as pedestal, gain, noise, linearity and saturation. Tuning of the performance can only be done globally for the SCA and not on individual pixels. Some of them exhibit anomalous behaviour, which is the subject of this paper. We address the phenomena of Random Telegraph Signal (RTS) noise, out-of-range baseline, anomalous baseline drift and high dark current. Identification of the latter three is also needed in order to correctly filter the RTS pixel population.

*ralf.kohley@esa.int

High Energy, Optical, and Infrared Detectors for Astronomy VII, edited by Andrew D. Holland, James Beletic,
Proc. of SPIE Vol. 9915, 99150H · © 2016 SPIE · CCC code: 0277-786X/16/$18 · doi: 10.1117/12.2233352

2. DEMONSTRATOR MODEL FOCAL PLANE ARRAY

The Demonstrator Model FPA (DM FPA) is composed of 2 SCA, 2 bare multiplexers, called "muxes" (CMOS ROIC without the hybridized HgCdTe layer) and 12 Structural and Thermal Model (STMs) arrays. The array assembly is shown in Figure 1 with its silicon carbide structure. The SCAs are identified as SCA1 and SCA2 for the analysis in this paper.

2 SCAs and the 2 muxes are positioned in diagonal into a 2x2 sub-array of the Focal Plane Array (Figure 1 right), mainly for compatibility tests performed on noise and dark current. The 4 arrays are controlled and read out by 4 SCEs, which are version B2 of the SIDECAR ASICs produced during the NRE Phase. The SCE is the cold front-end, which is connected to the Warm Electronics (WE) part of the detector system. For the DM the warm electronics is from Markury Scientific and consist of a set of custom boards:

- ACE cards (ASIC Control Electronic) which control up to 4 SIDECARs each
- MAICE card (Multiple ACE Interface and Control Electronics), which controls up to 8 ACE boards, provides power supplies, handles the data flow and provides a data acquisition interface via CameraLink.

The configuration for the DM FPA consists of a single ACE to read out 4 SCEs in parallel together with a MAICE, and provides a complete acquisition system in combination with a Matrox Frame Grabber located in a standard PCI-E slot. The Markury Scientific electronics is connected to the SCEs via 2 m long phosphor-bronze cables on loan from NASA GSFC DCL.

The original GUI provided with the hardware and running under Microsoft Windows 7 is mainly used for parameter control and configuration (power, power consumption, few ramps acquisition) of the ASICs connected to the ACE(s). Alternatively to this GUI, the system has been controlled by a set of Python code running under a Linux OS, using the Linux Version of the Matrox Imaging Libraries. This system, developed by the Euclid Consortium, provides a more robust working environment. It also has the advantage to directly write the raw data into a Hierarchical Data Format (HDF5) file. This structured file format allows for full compatibility to the analysis programs and avoids a painful and time-consuming conversion between different data formats. It also stores all metadata information from the test together with the raw data in form of a database.

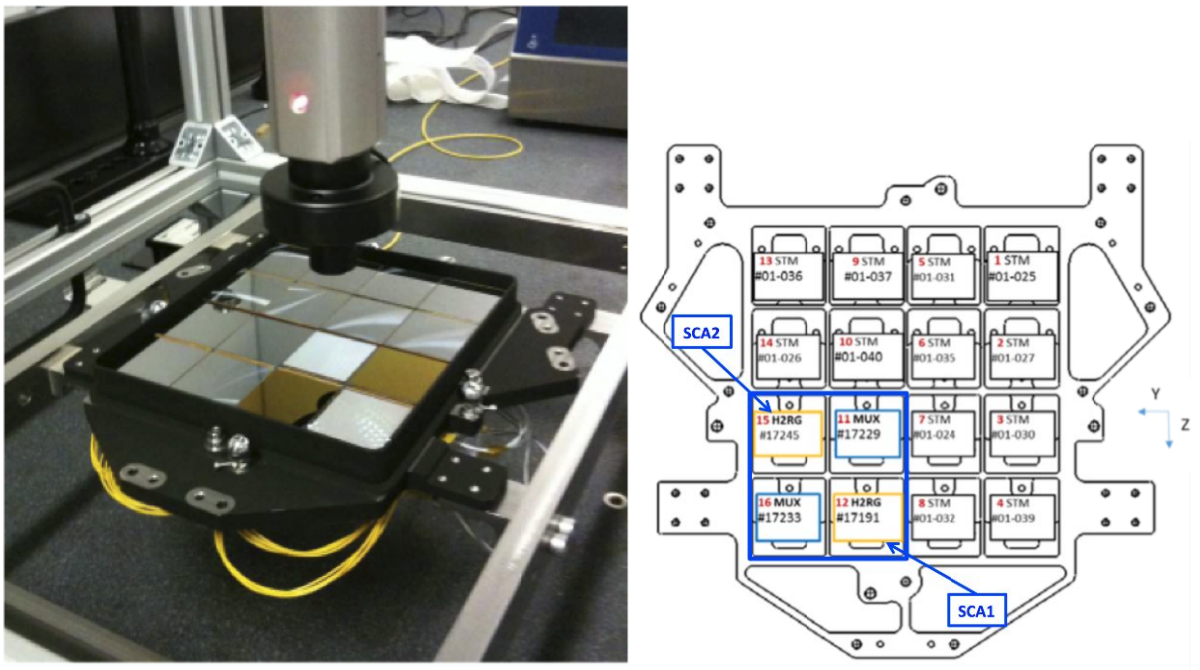

Figure 1: Setup of the Euclid Demonstrator Model (DM) FPA. Left: the frontside view of the assembled DM FPA with 12 STM (grey colour), 2 bare multiplexers (silver colour) and 2 NRE phase SCAs (darker colour), Right: FPA schematic (backside view) with indication of the SCA locations.

For the tests the DM FPA has been fully integrated into the instrument subsystem for the detection system, called NI-DS (see Figure 2 for a schematics of the full setup). This NI-DS demonstrator model has been installed into the LAM's NAC (Narrow Angle Camera, originally developed for the Rosetta mission) test facility in order to cool down and regulate the DM FPA at the required test operating temperatures via two bi-stage Sumitomo cryo-coolers. The facility provided a low noise and low thermal background environment for the tests.

The NI-DS has been operated at LAM over 10 full days during April 2015, allowing for about 6 full days of data taking in stable and dark conditions at 3 different operating temperatures of 80K, 90K and 100K, regulated at the cold support structure interface to the DM FPA. No major problem of acquisition has been found during these days and only 3 Cyclic Redundancy Check (CRC) errors have been noticed, each leading to a single unusable frame. Notice that more than 416000 frames (3.2 TB) have been acquired with different readout modes during the test campaign.

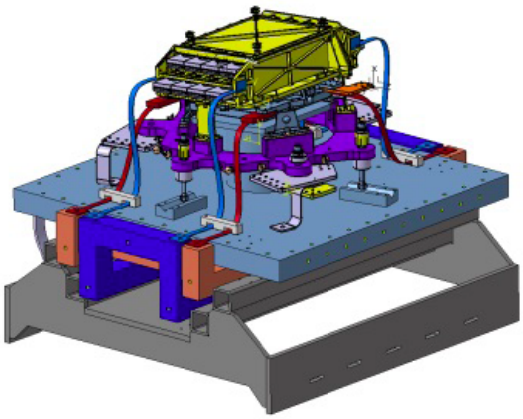

Figure 2: NI-DS test setup used for the Demonstrator Model tests of in April 2015. SiC structure holding the FPA in purple with SCE support in yellow with 2 rows of 4 SCEs (grey). The other structures in dark blue and red are copper thermal interfaces linked to the NI-DS via thermal braids (blue for the SCEs and red for the SCAs).

3. DATA ACQUISITION AND PROCESSING

3.1 Readout modes and configuration

The acquisition sequences during the tests were composed of:

- Short UTRs (Up The Ramp), 200 successive frames for quality checking purposes using a quick analysis.
- Long UTR ranging from 1000 to 20000 frames allowing to control system stability, and also the reconstruction of any other acquisition scheme (such as flight modes).
- Baseline acquisition (single frame acquisition preceded by reset) with changes of the reset voltage in order to compute the electronic gain and the thermal sensitivity of the electronic offset.
- Euclid flight scenarios for acquisition (sequences of photometry and spectrometry exposures with delays in between to mimic times needed for filter/grism wheel rotation and spacecraft activities to perform pointing dithers).

All readout modes can be expressed in form of Multi ACCumulation (MACC), which comprises 3 parameters to describe the acquisition process:

MACC(N,M,D) with N = number of groups, M = number of “read” frames per group (used for averaging), D = number of “drop” frames between groups (these are generated by the SCE but not sent to the warm electronics).

The Euclid flight scenario acquisitions used MACC configurations with 16 read frames and different number of groups and drop frames to accommodate the required exposure time. The baseline mode is a MACC(1,1,0) and a UTR of 5000 frames, which is the one we selected for the RTS noise analysis, is a MACC(5000,1,0). While not the longest ramp available with a complete set of frames, it was the most used during the tests, allowing for a good selection of suitable ramps.

The applied SCE gain were 18 dB leading to a conversion gain for both SCS (SCA1 and SCA2) of about 1.5 e-/ADU.

3.2 Raw data format and processing

Each frame of 2048 x 2048 pixels during the UTR 5000 is read out simultaneously over 32 channels, each corresponding to 64 columns. The image area photosensitive sites are the inner 2040 x 2040 pixels surrounded by a 4 pixel wide frame of reference pixels (4 column/rows left/right/up/down), which are used for reducing systematic noise components. An additional reference channel was also available, but the data from this channel has not used in the reference pixel subtraction scheme.

For the anomalous pixel behaviour different operations need to be performed on the individual frames of the UTR. Most are based on Correlated Double Sampling (CDS) in order to remove the electronic offset and its associated reset noise (kTC noise). The electronic offset, also called baseline or pedestal, is the inherent difference pixel-to-pixel of the reset level with a rather wide distribution spanning a few thousand ADU. The electronic offset cannot be independently tuned for each pixel and the common set point must be optimised to ensure good linearity and maximum dynamic range for the full array.

To support the following sections we define (N = 5000, i = 1..5000, j = 1..4999 for the UTR 5000):

Single frames:	Frame_i (Frame_1, …, Frame_N)
uCDS (UTR CDS):	uCDS_j = Frame_j – Frame_1
rCDS (rate CDS):	rCDS_j = Frame_(j+1) – Frame_j
Fowler-1:	fCDS = Frame_N – Frame_1

The single frames are used to identify out-of-range baseline (see section 4.2) and ADC saturated pixels. The uCDS or "up-the-ramp CDS" frames contain the signal as it integrates up during the UTR exposure. It usually contains the dark current ramp, signal jumps due to glitches (cosmic ray), etc. It is used to extract the timeline of signal values for the RTS noise analysis. The rCDS or "rate CDS" contains the signal increment from one frame to the next, e.g. normally the dark current rate for the frame time of 1.41s. Any jump in signal appears as a spike and it is used to count the number of transitions for the RTS noise analysis, the identification of pixels with high dark current rate and to evaluate the readout noise (CDS noise). The fCDS or Fowler-1 contains the integrated signal over the full ramp of 5000 frames, e.g. over the nearly 2 hours of exposure time for the UTR 5000.

All CDS frames are reference pixel corrected channel-to-channel through the up/down reference pixels and row-to-row through a sliding window of 9 rows on the left/right reference pixels.

4. ANOMALOUS PIXEL BEHAVIOUR

4.1 General considerations

The classification of certain pixel performances being anomalous is relative and measured against the statistical population and set minimum requirements on performance for the particular application. The affected performance parameters are the full scope of measurable parameters such as quantum efficiency, linearity, full well, gain, noise, electronic offset, dark current, persistence, etc. For example, a pixel with high dark current in excess of the minimum specifications might be flagged as "bad pixel" to be ignored in the data processing. Criteria were developed during the DM tests to generate these bad pixel maps for effects in darkness, namely dark current, noise and electronic baseline. Some of these are considered in the following sections. The concept of bad pixel or in general performance maps is also important in the context of defining operable pixels, e.g. pixels that fulfil the minimum performance requirements for a combination of parameters essential to achieve the required science return. In this paper we do not present the generated bad pixel maps and only address certain effects. Also the criteria and thresholds for bad pixels are adjusted to the case and needs of the RTS analysis and do not directly correspond to those needed for the Euclid mission. The RTS phenomenon may be treated as high noise, but due to the systematics could also lead to additional uncertainties in the signal ramp fitting. While we explain the phenomenon and quantify the parameter space, the assessment of the impact on science for Euclid is outside the scope of this paper.

4.2 Out-of-range baseline

As explained in section 3.2, the baseline set point is a trade-off considering the full distribution of the electronic offset for all pixels excluding outliers, which may have abnormally low or high baseline values. Some of these outliers may present baseline values at underflow or overflow (0 and 65535 ADU). This condition does not necessarily mean these pixels are "dead", only the baseline is outside the allowed range of the ADC. This has been seen on pixels with baseline 0 ADU that were illuminated and at one point during the up-the-ramp sampling entered the allowed ADC range and behaved like normal pixels.

Since the signal on these out-of-range baseline pixels cannot be recovered, these need to be flagged as bad pixels for the further analysis. Usually the population of out-of-range baseline pixels is quite limited and can be easily identified on the first frame after reset.

The consistent identification of these pixels on repeated baseline images is also needed to distinguish true pixels with overflow baseline from transient glitches (cosmic ray impact) that have occurred and saturated the pixel between reset and first frame acquisition. Another explication for recording 65535 ADU in a pixel on the first frame after reset would be very high dark current (leakage current) that again saturates the pixel between reset and first frame acquisition. ADC saturated glitches and dark current effects could be distinguished from baseline effects, if the full well capacity of the infrared diode under the applied reverse bias were below the ADC saturation limit.

Only 1 pixel on SCA1 was at 0 ADU baseline and none on SCA2. 844 pixels of SCA1 and 221 pixels of SCA2 show a baseline at 65535 ADU, therefore in total very few pixels are affected.

4.3 Baseline drift

Another phenomenon worth investigating is the baseline drift associated to instable bias supplies. While pixels with normal baseline behaviour show linear slopes additionally to the dark current contribution, some show instabilities or strong negative slopes. The drifts may show changing velocity and stabilize after a certain amount of time. Some examples are shown in Figure 3. To identify baseline drift pixels rate CDS images are analysed together with strong negative fCDS signal values. Positive linear baseline drifts can only be distinguished from dark current through temperature dependency, although we did not evaluate this in detail here, since the focus for this paper is on the RTS noise.

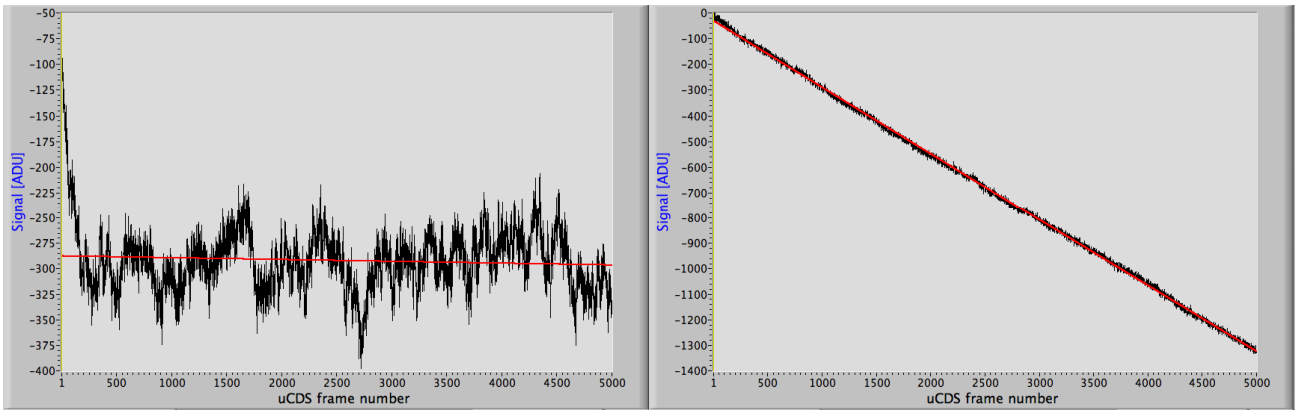

Figure 3: Two examples of baseline drifts on SCA1. (Left) the baseline is unstable with a large negative drift over the first 200 frames and then a changing drift pattern over the remaining frames. (Right) a strong negative linear baseline drift, which would correspond to a negative dark current of about -0.3 ADU/frame.

4.4 High dark current

Dark current is charge generated within the detector under absence of photocurrent. Dark current is a well-studied parameter in all types of detectors, because of its potentially large impact on science performance. In the Euclid SCAs the typical median dark current at the nominal operating temperature of 100K is expected to be very low. The measured median dark current on SCA1 during the DM tests was 0.018 e-/s and less than 0.032 e-/s for the 95%-tile (see Figure 4) and on SCA2 0.0077 e-/s with 0.021 e-/s for the 95%-tile. The dark current distribution over all pixels nevertheless shows a long tail towards high dark current values and pixels exceeding a threshold value of 0.2 e-/s were flagged as bad

pixels for this study. While linear dark current ramps will be subtracted off during the RTS noise analysis, the additional shot noise make these pixels less suitable for isolating the RTS and are therefore filtered out (about 5% of detected RTS candidates). Some ramps also show RTS in dark current (see Figure 5), but which was not further investigated statistically.

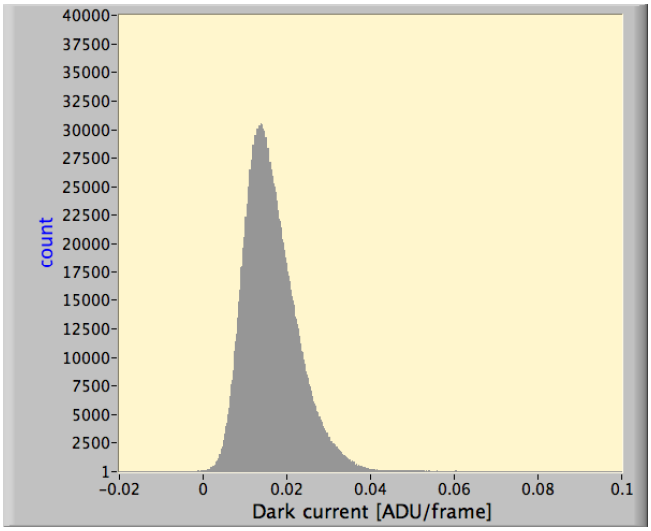

Figure 4: Distribution of dark current on SCA1 at 100K. Median dark current was 0.016 ADU/frame (0.0177 e-/s).

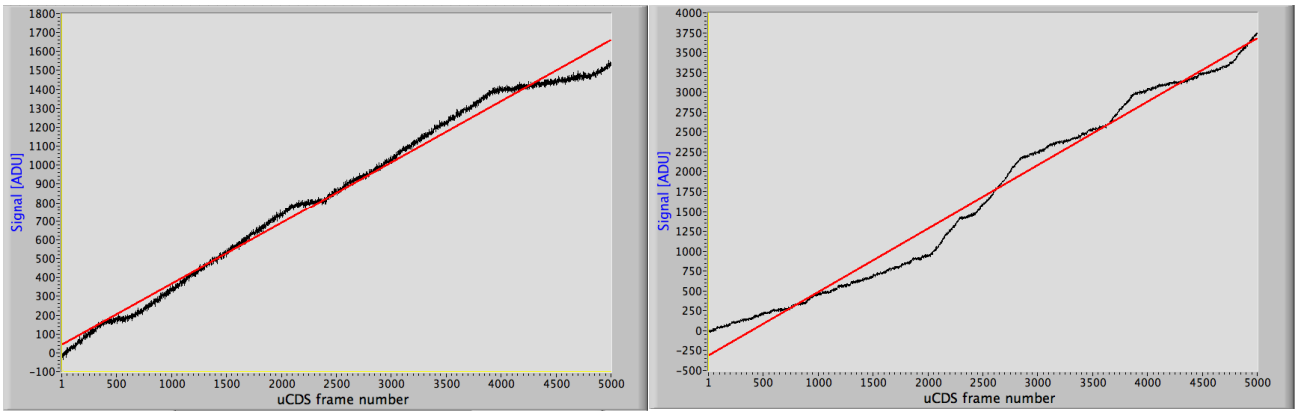

Figure 5: Two examples of dark current RTS. In both cases clearly the toggling between two distinct dark current generation rates are visible for these pixels on SCA1. The mean dark current generation as linear least-square fit is plotted as well for comparison.

4.5 Random Telegraph Signal

Random Telegraph Signal (RTS) is generally speaking the repeated change (or toggle) between two or more discrete states as systematic effect embedded in the signal. RTS can be associated to discrete changes of dark current rate in the semiconductor material (see Figure 5) or as RTS noise through discrete current changes in the on-chip amplifier structures. RTS noise has been studied in CMOS imaging sensors ([4], [5], [6]) and interpreted as trapping/de-trapping of interface states at the Si-SiO_2 interface of the source follower transistors. This mechanism also applies to the H2RG ROIC.

RTS noise (also called RTN) in the H2RG appears in form of spontaneous and discrete changes of baseline for individual pixels on frames acquired after a reset. The detection of the RTS noise is done on the long up-the-ramp sequences in the DM tests of 5000 frames. Initially the detection criterion was excess CDS noise and a high positive or negative maximum rate. Signal timelines (ramps) were created by subtracting each frame from the first frame after reset in order to remove the pedestal (UTR CDS, see section 3.2). Manual inspection of these single pixel signal timelines

showed that most RTS noise features were of two discrete states with different switching frequencies. The bi-state RTS can be described by three parameters:

(1) Amplitude: size of the transition step

(2) Period (inverse of toggle frequency): number of frames / number of transition pairs

(3) Average times in high (or low) state: number of frames in one or the other state / total number of frames

Following the trapping theory as origin for the RTS noise the average times in high and low state are related to capture and release time constants.

Examples of different RTS noise flavours are shown in Figure 6. These can be categorized into: (1) spikes and (2) square-wave transitions. Spikes are baseline excursions that immediately recover and can occur from very low (single spike) to very high frequency. Square-wave transitions are baseline excursions that stay in the opposite state for some time before switching back. Also here the frequency can be from very low (single transition) to very high. In both cases the high frequency RTS noise appears like normal noise, but presents two distinct value populations.

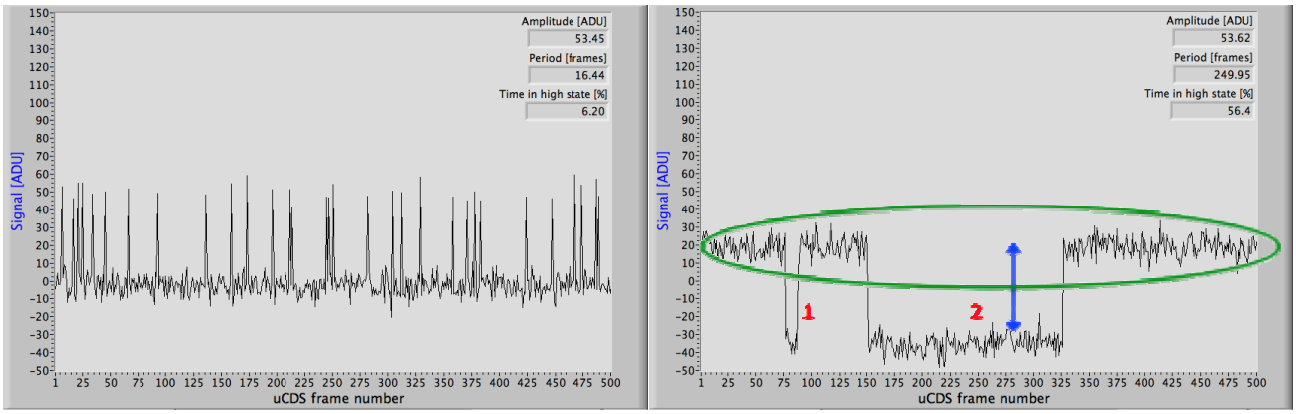

Figure 6: Two examples of RTS noise flavours. Dark signal ramps have been subtracted. Only the first 500 UTR CDS frames of the 4999 are shown for visibility: (Left) high frequency, spike-like baseline excursions. (Right) low frequency square-wave transitions with nearly equal time in high and low states. The characteristics leading to the three RTS parameters are marked on the plot to the right: amplitude (blue double arrow), number of transition pairs (2 in red, leading to period of 250 over 500 frames) and the frames related to time in high state (encircled in green).

5. RTS NOISE ANALYSIS

5.1 RTS noise detection algorithm

Given the discussions in the previous sections, the RTS noise analysis for the Euclid SCSs concentrates on the two-state RTS case. We opted for a signal value population based algorithm to detect RTS noise, as used by Bacon et.al ([7]). After dark ramp subtraction from the uCDS values, histograms are created in order to distinguish between noisy pixels (single peaked distribution) and two-state RTS (double peaked distribution). The histograms allow to recover the RTS noise amplitude and average time in high (or low) state (see Figure 7).

The transition amplitude is the difference between the Gaussian peak positions in ADU, e.g. the difference of the mean signal of the two value populations. The mean time in high (or low) state is the ratio of peak height divided by the sum of the peaks. In principle the integral should be taken, but under overlapping distributions the peaks are more robust and the width of the Gaussian distribution is assumed to be the same due to same readout noise, and any statistical spread in transition amplitude will affect both value populations. The missing parameter of RTS transition period is retrieved from the rCDS by counting the number of spikes and dividing the average of positive and negative transitions by the number of frames. Time in high state and period are not completely independent. If time in high state is very low (or very high) for a given period, the RTS is spike-like and if it approaches 50% square-wave-like, but for short period approaching 2 frames, the time in high state necessarily approaches 50% and no distinction between spike-like and square-wave-like can be made any longer (see Figure 12).

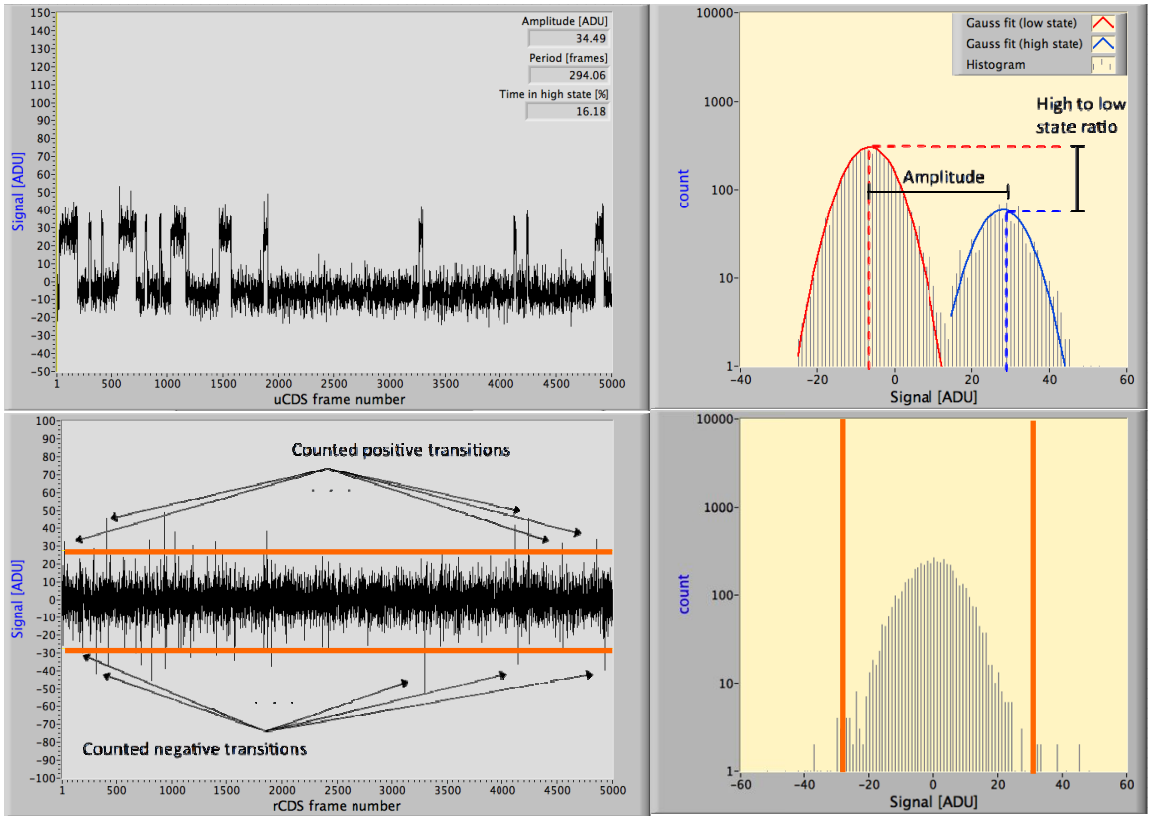

Figure 7: Example of RTS noise pixel analysis: (Upper left) Timeline of UTR CDS signal values. The analysis results are given as well. (Upper right) Histogram of the UTR CDS signal values. Two Gaussian envelopes have been fitted to the distributions belonging to the low and high states. The difference in Gaussian peak positions gives the estimate for the RTS noise amplitude. The peak heights are taken as measure for the time in high to low state ratio assuming similar distribution widths. (Lower left) the corresponding rate CDS values (differentiation of the upper left plot) and the estimated thresholds to count the number of positive and negative transition. These give an estimation of the RTS period. (Lower right) the histogram of the rate CDS values. The few and not spike-like transitions appear as outliers and not as separate populations like in the case of high frequency RTS.

5.2 Algorithm validation

The algorithm has been extensively validated with simulated data using 10000 Monte-Carlo runs each time with random setting of the three RTS parameters, a fixed readout noise of 10 ADU and a randomly chosen dark current slope from a normal distribution around the measured median dark slope during the DM tests. The simulations provided timelines of UTR CDS signal value in the range from 200 up to 5000 uCDS frames, which were analysed by the RTS noise detection algorithm, and results compared to the true simulated RTS parameter values.

The simulated amplitude range was initially set from 1 ADU to 300 ADU (see Figure 8). Nevertheless, below 30 ADU the algorithm can no longer distinguish true noise from small amplitude RTS and declares these cases as “no RTS”. Only about 9% of all simulated cases in the amplitude range from 1 to 30 ADU are detected as RTS. We therefore define a 30 ADU (~ 45e-) amplitude as the detection threshold and all further simulations were run for the amplitude range from 30 to 300 ADU. The chosen transition amplitude for one simulation is not taken as a fixed number for each triggered transition, but taken from a narrow normal distribution around the average input amplitude to allow for some statistical spread.

The range of period values depend on the number of frames and is set in between 2 frames and the number of frames in the UTR for the simulation. There is no fixed “beat frequency” implemented in the simulation, but the transitions between low and high state are triggered statistically based on the simulated period (see Figure 8 upper left plot for an example). The true simulated period is obtained by counting the number of commanded transitions. A higher density towards shorter periods (higher frequency) was chosen to reflect findings in manual inspection of RTS pixels.

Apart from the frequency, also the time in high state is statistically chosen in the simulations by modifying the probability on negative transitions with nearly equal distribution between 1 and 99%. The true simulated time in high (and low) state, which depends on the simulated frequency, is obtained by counting the number of frames in this state. The results from the simulations runs to validate the RTS noise detection algorithm are given below in Table 1.

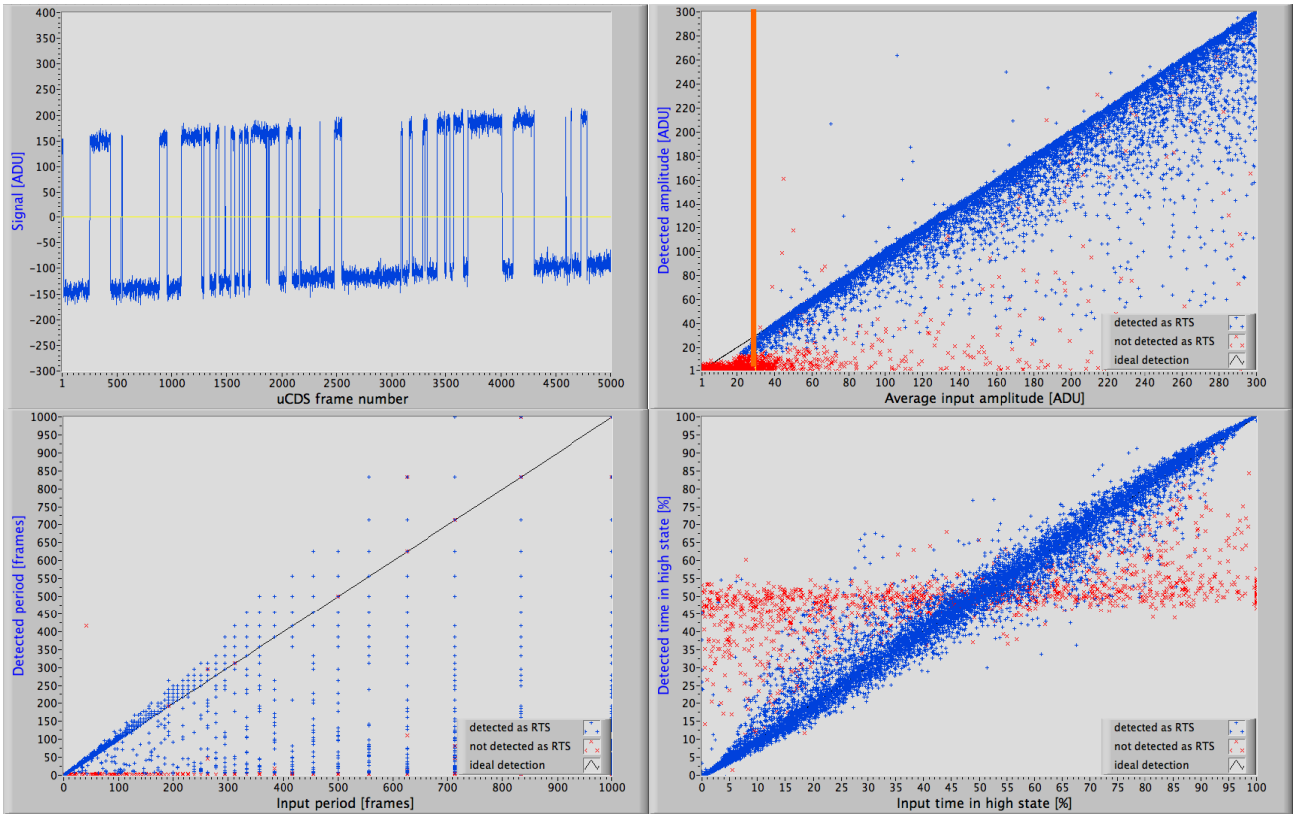

Figure 8: Example of simulation run: (Upper left) simulated timeline of a single pixel UTR CDS signal values over 5000 frames (dark current slope not subtracted). The simulation spans amplitude values from 0 to 300 ADU, periods from 0 to 5000 frames, time in high state from 0 to 100% and a readout noise of 10 ADU. (Upper right) efficiency diagram for amplitude. (Lower left) efficiency diagram for period. (Lower right) efficiency diagram for time in high state. Limiting the input amplitude to a minimum of 3-sigma CDS noise (30 ADU, see vertical bar in upper right plot), the repeatability of parameter recovery is +/-15% for more than 80% of the cases.

Table 1: RTS detection and parameter value determination performance of the algorithm on simulated data

Number of frames	RTS detection Efficiency	RTS detection Purity	Amplitude recovery success [+5%, -15%]	Period recovery success [+15%, -5%]	Time high state recovery success [+10%, -10%]
200	43%	89.5%	30%	85%	36%
1000	78%	99.9%	53%	81%	49%
2000	86.5%	100%	68%	83%	58%
2500	89.5%	100%	72%	84%	61%
5000	95%	100%	83%	85%	71%

Another question to solve was the amount of frames needed for the RTS analysis. In the simulation this was expressed as efficiency (number of true positives / number of true RTS) and purity (number of true positives / (number of true positives + number of false positives)). The false positives were assessed through using pure noise instead of RTS input signals in the simulations. Table 1 summarizes the results. The parameter recovery success rates are against the true

simulated parameter value within the given error interval of 20%. The high success rate for period recovery is biased by the higher density of shorter periods in the simulations, which are recovered with a higher success rate than the longer periods.

Based on the simulation results and the availability of several UTR 5000 data sets from the DM tests, the number of processed frames was set to 5000. While the simulation results are promising, care needs to be taken to not rely on detection and parameter success rates for single UTR 5000 ramps of the true test data, since residuals for example from reference pixel corrections and low frequency noise were not accounted for in the simulations. Also the true parameter value distributions were only based on limited manual inspections of RTS pixels, and would need to be revised.

Moreover the recovery for large period RTS is not as good as hoped for, partly because of robustness concerning the dark current ramp subtraction, which may spoil the value population histograms and give erroneous results. This is an area where the algorithm would need improvement together with lowering the detection threshold to lower amplitude RTS.

5.3 Results

The algorithm was run on the available UTR 5000 ramps for both SCS and at different operating temperatures. Several ramps at the same temperature and for the same SCS are used to crosscheck the obtained results for consistency. Furthermore individual pixels were inspected to verify the correct execution of the algorithm. Table 2 give the summary of the used data sets. During some ramps not all SCS were switched on. The data sets corresponding to either SCA1 and/or SCA2 are indicated in the table. In total 9 UTR 5000 ramps were processed, 5 for SCA1 and 4 for SCA2.

Table 2: Processed UTR 5000 ramps from the DM tests

Data set	Date / time	SCA1	SCA2	Operating temperature
1	20150419_06h59_36	Yes	-	90 K
2	20150419_08h57_54	Yes	-	90 K
3	20150419_11h00_50	-	Yes	90 K
4	20150419_13h00_21	Yes	Yes	90 K
5	20150420_22h02_17	Yes	Yes	100 K
6	20150421_00h09_54	Yes	Yes	100 K

The algorithm works unbiased and determines for each pixel the parameters based on the histogram and rate CDS analysis. The results are stored in image files of the same dimension as the UTR frames. Additionally and based on the criteria described in section 5.1, the suspected RTS pixels are flagged and stored as a bit map, which can be used to filter the RTS candidates for further analysis.

5.3.1 Count rates and 2D distribution

Even filtering out other anomalous pixels (see sections 4.2, 4.3 and 4.4) by applying the corresponding selection maps, the RTS detection efficiency is not 100% (see Table 1) and rapidly drops for low amplitude RTS, which on some ramps might be detected as RTS and on others not. Furthermore glitches (cosmic ray impacts) occur at random locations during the UTR integration and can be mistaken as RTS. Therefore we take a minimum of 2 UTR to exclude random events and to consolidate a list of true RTS pixels. In the selection of the UTRs for this analysis we have ensured that this is the case for each SCS and operating temperature (see Table 2). The combined maps are a logical AND of the individual bitmaps. The number counts are presented in Table 3.

The amount of rejected RTS candidates when combining the information from two ramps initially looked very high, but further inspection showed that most of them indeed were glitches causing a positive jump over the ramp of 5000 frames. If most of the rejections were attributed to glitches, the rate would be around 2 affected pixels per second.

In all cases the consolidated number of RTS pixels is below 1% of all image area pixels. RTS pixels are also found among the reference pixels with approximately the same fraction. This confirms the origin of the RTS to be within the ROIC. The detected number of RTS depends heavily on the detection threshold of the used algorithm and not detected low amplitude RTS might increase this number substantially (see Figure 9). One could even suspect that the population

of RTS seamlessly blends into the true noise towards small amplitudes and that in a way all pixels are RTS, but this is mere speculation. On the other hand, RTS with smaller amplitude will also certainly have a smaller or even negligible impact on science apart from the noise contribution. The histogram in Figure 9 shows that amplitude is very contained with 95% of detected pixels with amplitudes below about 300e- (200 ADU) for both SCA and temperatures.

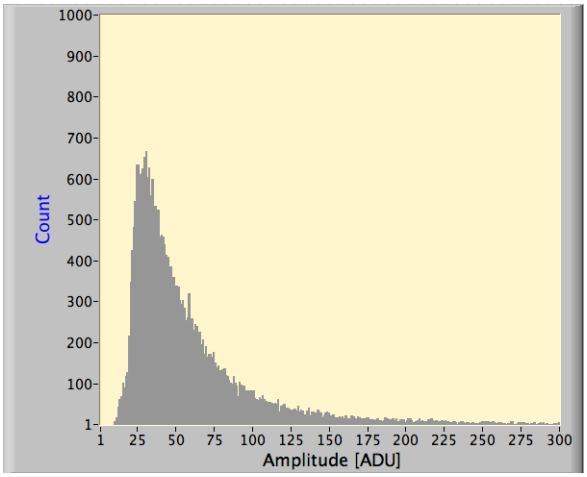

Figure 9: Histogram of amplitude value distribution for SCA1 and 90K. The drop in number counts below about 30 ADU is heavily conditioned by the detection threshold of the algorithm, which is in this order (see section 5.2). Completeness falls off and if the detection threshold could be reduced, the count rate for smaller amplitudes might still raise as assumed from higher amplitude counts.

Table 3: Number of identified RTS candidates and consolidated lists

SCA	Operating temperature	Data sets	RTS candidates (image area pixels)	RTS candidates (reference pixels)
SCA1	**90K**	1	45235	340
		2	45358	352
		4	46320	342
		Combined (1, 2)	**31134**	**261**
		Combined (1, 4)	**30972**	**257**
		Combined (2, 4)	**31286**	**262**
		Combined (1, 2, 4)	**28163**	**227**
SCA1	**100K**	5	43089	252
		6	45118	258
		Combined (5, 6)	**28533**	**204**
SCA2	**90K**	3	52581	412
		4	53922	414
		Combined (3, 4)	**39508**	**345**
SCA2	**100K**	5	46519	323
		6	50317	313
		Combined (5, 6)	**32376**	**259**

Combining found RTS pixels on the same SCA for different temperatures show a drastic drop in count numbers, which might be due to changed parameters and population under temperature changes (see section 5.3.4).

An interesting point to look at is the spatial distribution of the consolidated list of RTS pixels. A view of the distribution is shown in Figure 10. For both SCS and both operating temperatures the RTS pixels were nearly homogeneously distributed.

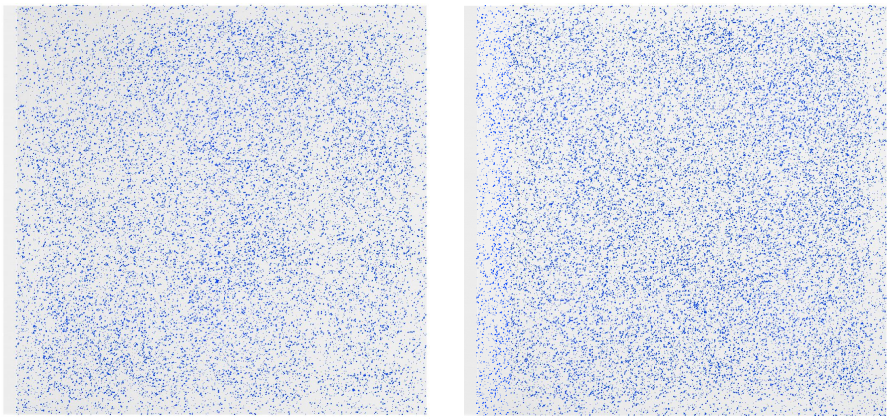

Figure 10: Location of detected RTS pixels on SCA1 (left) and SCA2 (right). The RTS pixels are homogeneously distributed over the image area. The reference channel on the underlying images is located to the left and not relevant for this analysis.

5.3.2 Repeatability of RTS parameter value extraction

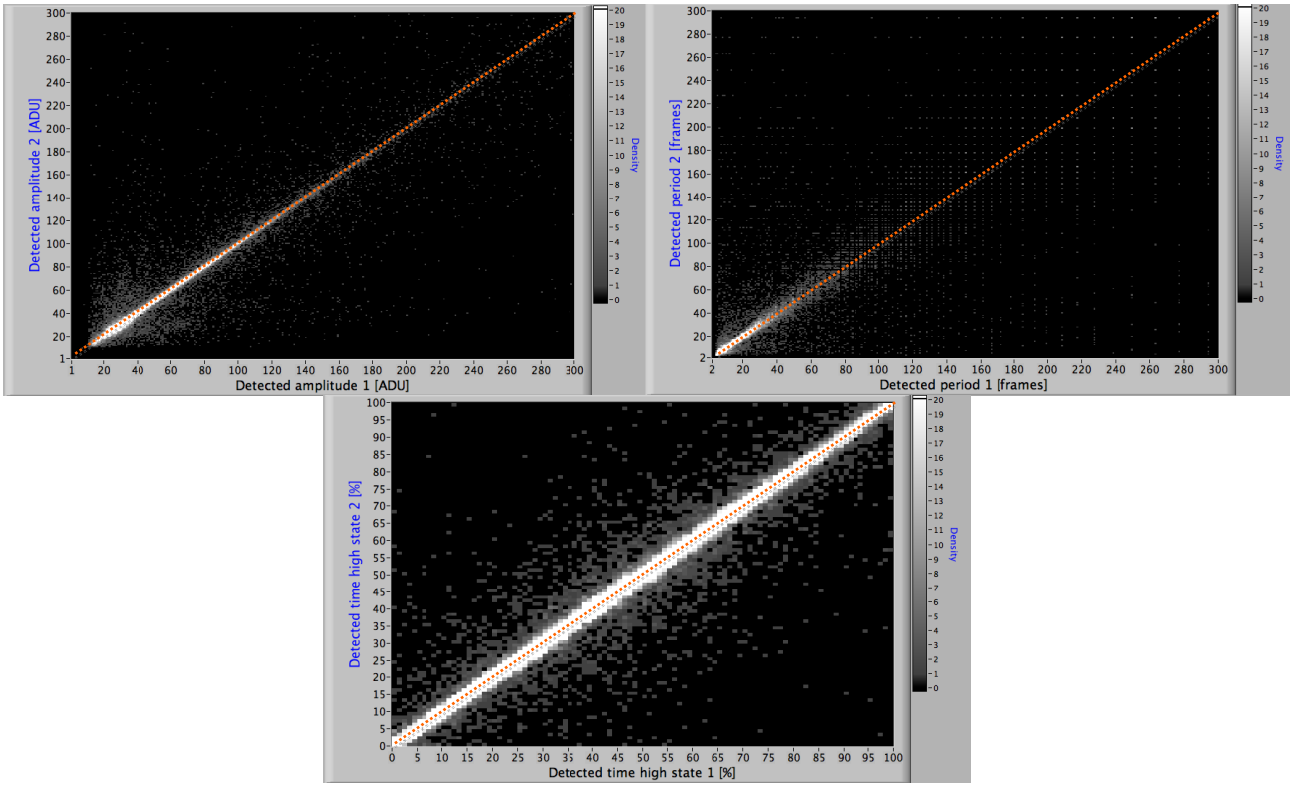

Figure 11: Intensity plots of correlation between the detected RTS parameter value in one data set with respect to another (for the same RTS pixel) in the list of consolidated RTS pixels. As an example the case of SCS2 at 90K is shown. For the three parameters the repeatability within an error of 20% is more than 90% of RTS pixels for amplitude, more than 85% for period and more than 90% for time in high state, fully in line with expectations from simulations. The ideal correlation line is plotted as well as dashed line.

In order to check the repeatability of RTS parameters value recovery, correlation plots were produced between each of the two data sets used to generate the consolidated list of RTS pixels. In these plots the parameter values for the same RTS pixel of one data set are plotted against the corresponding values in the other data set. The error is evaluated as distance from the ideal correlation line, and in all cases and for all parameter values is found to be fully in line with expectations from the simulations. This confirms that the algorithm works consistently to this level of precision. Intensity diagrams that show the correlation between the detected parameter values are shown in Figure 11 on the example of SCS2 and 90K.

The underlying assumption is that the parameter values of a certain RTS pixel under the same operating conditions are invariant and not changing from one UTR ramp to the next.

5.3.3 RTS noise flavour preference

Correlation plots can also be built for different parameters and the same data set to visualise the preferred RTS parameter combination out of the pool of detected RTS pixels. The analysis shows that the majority is of a spike-like nature with preferred tendency to small periods and amplitudes. Figure 12 shows these correlations on the example of SCS2 and 90K operating temperature.

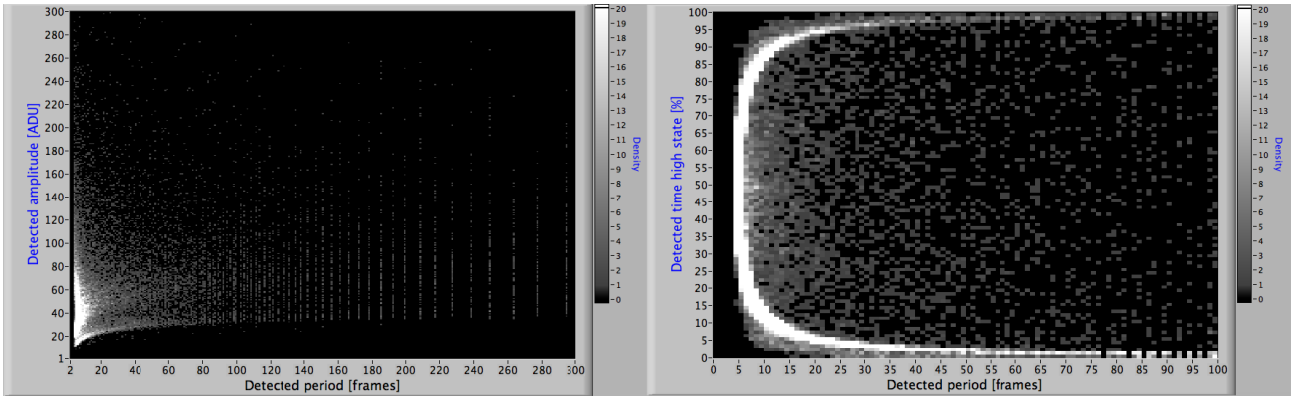

Figure 12: Intensity plots of (left) correlation between detected period and amplitude for the same data set and (right) the same for the correlation between period and time in high state. These correlation plots show that the majority of RTS pixels have small periods, rather small amplitudes (the latter limited by detection threshold towards very small amplitudes) and in general tend to be of the spike-like type. On the right hand side plot the time in high state is of course dependent on the period, necessarily going towards 50% for periods approaching 2 frames.

5.3.4 Temperature dependence

To understand the temperature dependency both statistically and on examples the data sets for two different temperatures of 90K and 100K for both SCA1 and SCA2 were analysed. Combining the RTS candidate flag maps for both temperatures, the combined map has only half of the number count of that of the individual temperatures or about 16000 detected RTS (see Table 3 for comparison), which was not expected and still is being investigated. On the commonly identified RTS pixels the statistical analysis shows that amplitude is slightly reduced for 100K with respect to 90K and that the period is drastically reduced (see Figure 13). The time in high state is connected to the change in period.

A selection of individual pixels were inspected for both the group of commonly detected RTS candidates for both temperatures, and those, which were detected in the data set of one temperature but not in the other. In many cases the increased frequency (reduced period) is confirmed (see Figure 14 for an example). There are also some cases, where pixels seem to develop RTS at higher temperature. This could be though an artefact considering a very low frequency RTS behaviour at 90K, which simply did not present any transitions during the 5000 frame ramps (see Figure 15). Considering trapping/de-trapping as the origin of the RTS phenomenon, a higher frequency at higher temperatures would be expected due to the reduced trap release times.

The exact RTS properties and population changes with temperature and under thermal cycles needs further study and will be done once test data from dedicated runs for this purpose are available.

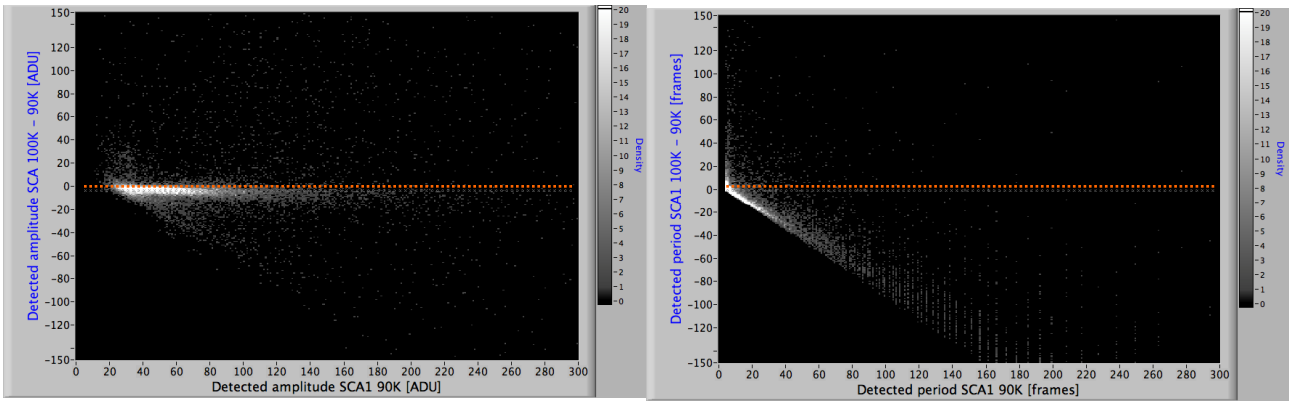

Figure 13: Intensity plots of (left) correlation between detected amplitude for the same SCA and the same pixels, but under the two different temperatures (90K and 100K), and (right) the same for the correlation concerning period. The y-axis shows the difference of the 100K to 90K case in detected amplitude and period. The plots show that amplitude is slightly reduced for 100K with respect to 90K and period statistically is much reduced for 100K. The ideal correlation line is plotted as well as dashed line.

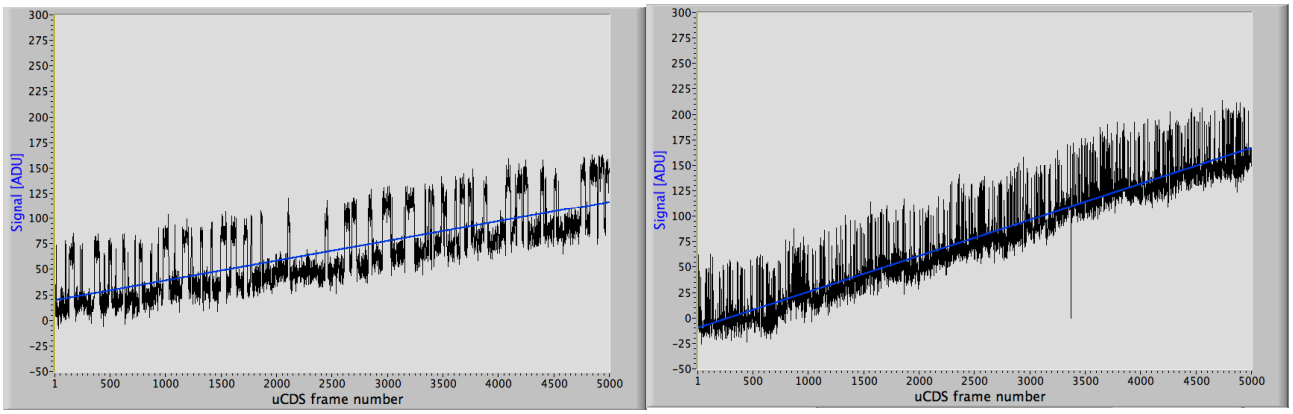

Figure 14: UTR CDS timelines for the same RTS pixel on SCA1 at the operating temperature of 90K (left) and 100K (right). The increase in dark current slope (linear least-square fit added as blue line) due to the increased temperature is clearly visible as well the increased frequency (shorter period) for the 100K case.

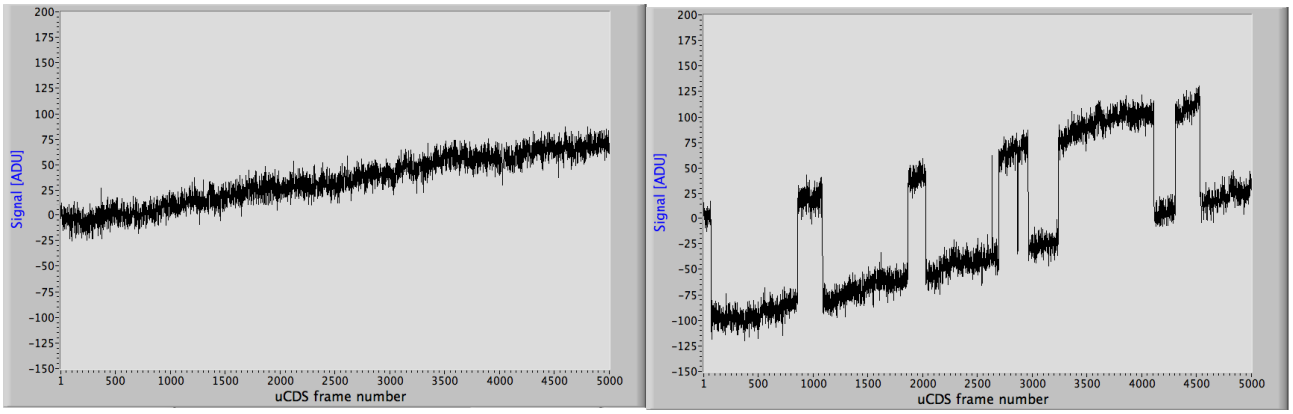

Figure 15: UTR CDS timelines for the same pixel on SCA1 at the operating temperature of 90K (left) and 100K (right). While at 90K no RTS signature can be detected, it is clearly visible at 100K.

6. CONCLUSIONS

Different types of anomalous pixel behaviour in darkness have been presented with special focus on the RTS noise phenomenon in form of spontaneous baseline changes during the up-the-ramp integration seen as toggling between two discrete states. An algorithm has been implemented to detect RTS noise candidates unbiased in the available data sets from the demonstrator model tests of the Euclid FPA on two pre-development Teledyne HgCdTe H2RG 2.3µm cut-off detector systems custom-made for the Euclid mission.

Validation of the algorithm has shown that the detection threshold is at about 45e- (about 3-sigma CDS noise), which limits the completeness of low amplitude RTS. The existence of these low amplitude RTS has been identified by eye on individual pixels, but only for low frequency cases. It is speculated that there might be a seamless transition between low amplitude RTS noise and normal noise, which would make the RTS phenomenon common and not reduced to isolated cases. Improvements to the detection algorithm performance to smaller amplitudes are needed to prove this statistically, which is planned for a future study. With the current detection threshold the number counts of RTS pixels are less than 1% of all pixels with same proportions for the photosensitive image area pixels as well as for the reference pixels, which confirms the origin in the H2RG ROIC.

In general the RTS behaviour in the detected RTS pixels is spike-like rather than square-wave-like with tendency to higher frequencies, e.g. smaller period, and small amplitudes. While isolated cases with higher amplitudes were detected, 95% of all detections showed amplitudes smaller than about 300e-.

The temperature dependency of the RTS behaviour has been investigated as well showing in general slightly smaller amplitudes and much shorter periods (higher frequency) when going from 90K to 100K operating temperature. The higher frequency at higher temperature would be expected considering the trapping/de-trapping origin of the RTS phenomenon due to reduced trap release times. Further studies of RTS behaviour change under temperature changes are needed though to fully understand the dependency. Open questions that still could not be addressed through the FPA DM test data are any changes to the RTS population and properties under thermal cycles, and especially under the influence of radiation damage, which will be carried out once the dedicated test data is available.

REFERENCES

[1] Racca, G., et al., “The Euclid mission design”, Proc. SPIE 9904, (2016)
[2] Maciaszek, T., et al., “Euclid Near Infrared Spectro Photometer instrument concept and first test results at the end of phase C”, Proc. SPIE 9904, (2016)
[3] Clémens, J. C., et al., “EUCLID detector system demonstrator model: a first demonstration of the NISP detection system”, Proc. SPIE 9602, (2015).
[4] Woo, J.M., Park, H.H., Hong, S.M., Chung, I.Y., Min, H.S., Park, Y.J., “Statistical Noise Analysis of CMOS Image Sensors in Dark Condition”, IEEE Transactions on electron devices, Vol 56 N° 11, 2481 (2009)
[5] Martin-Gonthier, Ph., Magnan, P., “RTS Noise Impact in CMOS Image Sensors Readout Circuit”, 16th IEEE International Conference on Electronics, Circuits, and Systems (ICECS), 928-931 (2009)
[6] Goiffon, V., Magnan, P., Martin-Gonthier, Ph, Virmontois, C., Gaillardin, M.. “New source of random telegraph signal in CMOS image sensors”, International Image Sensor Workshop (Hokaido, Japan), (2011)
[7] Bacon, C., et al., “Burst Noise in the HAWAII-1RG Multiplexer”, Proc. SPIE 5902, (2005)